Self-Assembly of Colloidal Molecules due to Self-Generated Flow

Ran Niu (牛冉), Thomas Palberg, and Thomas Speck
Institut für Physik, Johannes Gutenberg-Universität Mainz, Staudingerweg 7-9, 55128 Mainz, Germany
(Received 23 February 2017; revised manuscript received 19 May 2017; published 11 July 2017)

The emergence of structure through aggregation is a fascinating topic and of both fundamental and practical interest. Here we demonstrate that self-generated solvent flow can be used to generate long-range attractions on the colloidal scale, with subpiconewton forces extending into the millimeter range. We observe a rich dynamic behavior with the formation and fusion of small clusters resembling molecules. The dynamics of this assembly is governed by an effective conservative energy that for large separations r decays as $1/r$. Breaking the flow symmetry, these clusters can be made active.

DOI: 10.1103/PhysRevLett.119.028001

Colloidal particles acting as "big" artificial atoms have been instrumental in studying microscopic processes in condensed matter, from the vapor-liquid interface [1] to the kinetics of crystallization [2]. Because of their size, colloidal particles are observable directly in real space. Moreover, interactions are widely tunable, ranging from hard spheres to long-range repulsive, short-range attractive, and dipolar [3,4]. Consequently, colloidal particles can be assembled into a multitude of different structures: from clusters [5–7] and stable molecules [8,9] composed of a few particles to extended bulk structures like ionic binary crystals [10]. In addition, self-assembly into useful superstructures can be controlled by factors such as confinement [11] and particle shape [12], which make colloids a versatile and fascinating form of matter [13].

What is still missing is truly long-range attractions of like-charged (or uncharged) identical colloidal particles. There is much interest in the basic statistical physics of systems with such interactions, which play a role in gravitational collapse, two-dimensional elasticity, chemotactic collapse, quantum fluids, and atomic clusters [14]. One proposed realization is colloidal particles trapped at an interface [15] that experience screened, long-range attractions due to capillary fluctuations of the interface [16,17]. The attractive interactions then correspond to Newtonian gravity in two dimensions. Magnetic and electric dipolar interactions decay as $1/r^3$ and lead to interesting phase behavior [18,19]. Complex patterns are also known to arise for bacteria due to long-range chemotactic interactions [20]. Critical long-range Casimir forces have been reported for colloidal particles in a binary solvent [21], which are tunable by temperature and surface chemistry. Finally, a recent theoretical proposal is catalytically *active* colloidal particles that interact through producing or consuming chemicals [22,23]. For simple diffusion, the concentration profile of a chemical decays as inverse distance, implying long-range interactions that can be tuned through activity (how chemicals are produced or consumed) and mobility (how particles react to gradients).

Here, we implement long-range attractions through hydrodynamic flows coupling suspended particles [24,25]. We report on experiments using spherical ion exchange resin particles sedimented to the negatively charged substrate. The particles have diameters of 15 μm, for which Brownian diffusion is practically negligible on the experimental time scale. They interact due to self-generated local *flow*, resulting in an effective long-range $1/r$ attraction as expected for three-dimensional unscreened gravity. Our present understanding of the mechanism responsible for their aggregation can be summarized as follows [26,27]: By exchanging residual cationic impurities for stored hydrogen ions [Fig. 1(a)], the particles generate a concentration profile c that decays away from the particles. Different diffusion coefficients of the exchanged cations and the released ions locally generate diffusio-electric fields which retain overall electroneutrality by slowing the outward drift of hydrogen ions and accelerating the inward drift of impurities.

The total system composed of solvent, ions, and colloidal particles is clearly out of thermal equilibrium through the free energy released by solvating the hydrogen ions, which drives the flow. However, appealing to a scale separation between particles and solvent, our crucial assumption will be that the motion of the particles themselves can be described by

$$\dot{\mathbf{r}}_i = -\nabla_i U + \boldsymbol{\eta}_i, \tag{1}$$

where $U = \sum_{i<j} u(\mathbf{r}_i - \mathbf{r}_j)$ is a conservative potential, $u(r)$ is the pair potential Eq. (2), and $\boldsymbol{\eta}_i$ models noise with zero mean and correlations $\langle \boldsymbol{\eta}_i(t)\boldsymbol{\eta}_j^T(t')\rangle = 2D_{\mathrm{eff}}\mathbf{1}\delta_{ij}\delta(t-t')$. This noise is not thermal but arises from fluctuations of the induced flow. Usually, overdamped motion is described by a product of particle mobility and the gradient of the potential energy. Since we do not have access to these terms separately, we treat $u(r)$ as an effective "energy" absorbing the phoretic mobility μ, with $u(r)$ thus having units of a diffusion coefficient.

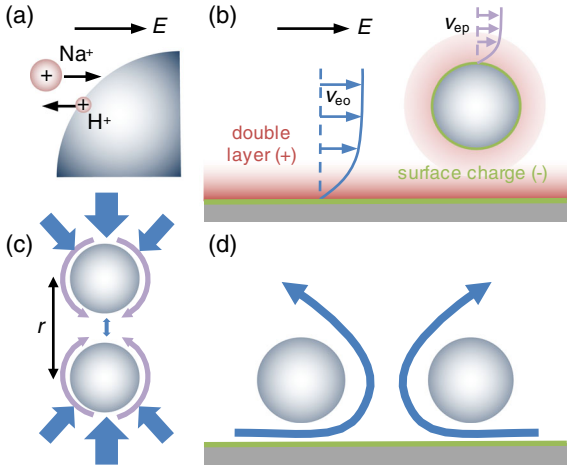

FIG. 1. Long-range interactions through flow. (a) The colloidal particles release hydrogen ions (H^+), which are exchanged with residual cationic impurities (here Na^+). Different ion mobilities generate local electric fields E that slow the hydrogen ions and accelerate the impurities to maintain overall electroneutrality. (b) In the double layer of the substrate, these fields generate electro-osmotic flow with solvent velocity v_{eo} towards the particle. In the double layer of the particles, the electric fields lead to electrophoretic flow. (c) Top view of the flow geometry: For two particles a distance r apart, the higher H^+ concentration in the space between particles reduces the gradient and leads to an asymmetric electro-osmotic flow and thus attraction. (d) Side view sketching the flow away from the substrate.

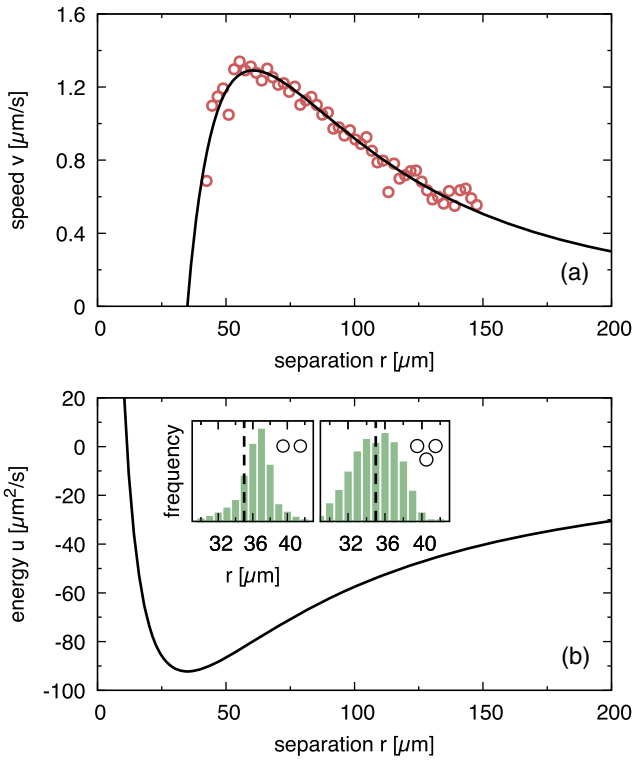

FIG. 2. Effective pair potential. (a) Drift velocity $v(r)$ of two particles with separation r (symbols). The line is the free fit to $v(r) = 2u'(r)$ with $u'(r)$ denoting the derivative of Eq. (2). (b) The resulting effective pair potential $u(r)$. Insets: Histograms of the fluctuating bond length of dimers (left) and trimers (right), where the dashed line indicates the minimum $r_0 \simeq 35$ μm of the fitted effective potential.

The relative velocity of two particles with separation $\mathbf{r} = \mathbf{r}_1 - \mathbf{r}_2$ is $v(r) = \langle(\mathbf{r}/r)\cdot(\dot{\mathbf{r}}_1 - \dot{\mathbf{r}}_2)\delta(|\mathbf{r}| - r)\rangle = 2u'(r)$ after inserting Eq. (1). Hence, we have direct access to the interactions $u(r)$ through measuring a dynamic quantity, the approach velocity $v(r)$ as shown in Fig. 2(a). Approaching each other, the speed increases as expected but reaches a maximum at about $r \simeq 60$ μm before it drops rapidly.

This behavior can be rationalized by considering the generated flows in more detail. In the double layer of the substrate, the local fields generate electro-osmotic flow of the solvent, since the negatively charged substrate is screened by an excess of positive charges [Fig. 1(b)]. For an isolated particle, the solvent flow is approaching symmetrically and no net motion results (the particle can be regarded as a sink in two dimensions). For two particles, the hydrogen ion concentration is increased in the space between the particles, which reduces the gradient and thus the flow velocity. Hence, the flow on each particle now becomes asymmetric, resulting in an apparent attraction [Fig. 1(c)]. Of course, the solvent is incompressible with backflow out of the plane of the substrate [Fig. 1(d)].

In addition, the fields generated by the second particle lead to electrophoretic flow, since the particles themselves are (slightly) negatively charged due to the release of cations. Since now the particle and solvent taken together are force-free, the particle moves in the *opposite* direction of the field. Electrophoretic flow is determined by the slip velocity $v_{ep} = -\mu_p \nabla c$ with ion concentration field c and phoretic mobility μ_p [26], whereby our measured particle velocities are consistent with a constant mobility. For purely diffusive ion motion, one would expect the concentration to decay as $c(r) \sim 1/r$, but measurements of the pH reveal a more complicated behavior [these measurements had to be performed for a larger particle (see Supplemental Material [28]), but we expect the qualitative features to be the same for the smaller particles used here]. While there is indeed a $1/r$ decay regime, closer to the ion exchange particle it changes to a regime that is well described as exponential. We speculate that this accumulation is caused by the local fields slowing down outward moving ions.

For large separations r we thus observe attraction due to the electro-osmotic flow along the substrate, while for small separations a combination of electrophoretic and out-of-plane flow will lead to a repulsion. We model the latter through a term resembling screening, although we stress that it originates from the flow and not electrostatics. Combining both effects, the functional form of the potential reads

$$u(r) = -\frac{\gamma}{r} + \frac{\alpha}{r} e^{-r/\xi} \qquad (2)$$

with three free parameters: the prefactors γ and α and the screening length ξ. As shown in Fig. 2(a), this function describes the experimental data very well. From the fit we obtain $\gamma \simeq 6120\,\mu\mathrm{m}^3/\mathrm{s}$, $\alpha \simeq 8805\ \mu\mathrm{m}^3/\mathrm{s}$, and $\xi \simeq 31.4\ \mu\mathrm{m}$. The pair potential $u(r)$ plotted in Fig. 2(b) has a minimum at $r_0 \simeq 35\ \mu\mathrm{m}$. As shown in the inset in Fig. 2(b), r_0 agrees well with the maximum of the distributions of bond length r for dimers and trimers. To estimate the physical energies, we employ the bare particle mobility μ_0, which quantifies the forces needed to move a single particle through the solvent with the desired speed. For our particles in water, its value is $\mu_0 \simeq 7.8\ \mu\mathrm{m}/(\mathrm{s}\cdot\mathrm{pN})$, yielding forces between particles of the order of 0.1 pN. With $u(r_0) \simeq -92.34\ \mu\mathrm{m}^2/\mathrm{s}$, the corresponding bond dissociation energy would thus be $E_b = |u(r_0)|/\mu_0 \simeq 7000\ \mathrm{kJ/mol}$.

The final ingredient for our theoretical model is an effective temperature, which we extract from the measured bond fluctuations. First, from the distribution of the bond length r for dimers, we determine its variance $\mathrm{Var}(r) \simeq 3.57\ \mu\mathrm{m}^2$. Assuming that these vibrations are effectively equilibrated allows us to determine the analog of a temperature, $D_{\mathrm{eff}} \approx \mathrm{Var}(r)u''(r_0) \simeq 0.3\ \mu\mathrm{m}^2/\mathrm{s}$. We test this assumption for three particles, for which a quick calculation predicts that the harmonic bond fluctuations are $\frac{5}{3}$ times larger [28]. The predicted value $5.95\ \mu\mathrm{m}^2$ is only slightly smaller than the measured variance $6.25\ \mu\mathrm{m}^2$.

Our suspension of ion exchange particles is not stationary but slowly collapses to a close-packed state due to the long-range interactions. During this process, the flow remains unaltered, lasting for about 7 h [28]. Starting from a homogeneous density profile, we observe the formation of colloidal clusters ("molecules") with n particles. This assembly happens autonomously in contrast to prefabricated colloidal molecules [30,31]. Although being metastable, single clusters can be observed up to minutes, which allows one, in principle, to study in detail different isomers and the "reactions" by which larger clusters form (more details are given as Supplemental Material [28]). In Fig. 3(a), we show the first few minutes of this process for a dilute suspension. The experiments were carried out with 60–90 particles within a field of view corresponding to an area fraction of approximately 0.25%. Without adjustable parameters, the observed dynamics are reproduced through the model described by Eq. (1). In Fig. 3(b), we show a sequence of experimental snapshots for seven particles. We then perform simulations of the model using the extracted particle positions from the first experimental frame as initial positions. As shown in Fig. 3(c), the simulations agree with the experiments on the same time scale. Whereas for repeated simulation runs the positions differ due to the noise, the average behavior is consistent.

This fit-free quantitative agreement is corroborated by the time evolution of the fraction of clusters with weight n. From the analysis of the experiments, we extract the fraction $N_n(t)/N$ of particles residing in clusters with n particles. The range of N is between 60 and 90, and to improve statistics we average over all experiments. We repeat the same analysis with the theoretical model for $N = 80$, the comparison of which is shown in Fig. 4. The qualitative behavior is that of irreversible aggregation as described through the Smoluchowski coagulation equation [32], with a steady decrease of the monomer concentration and peaks for the n-mers that become flatter and shifted to later times for increasing weight n.

As demonstrated, for a one-component suspension of ion exchange particles in moderate flow, the dynamics of the particles alone is effectively described through a

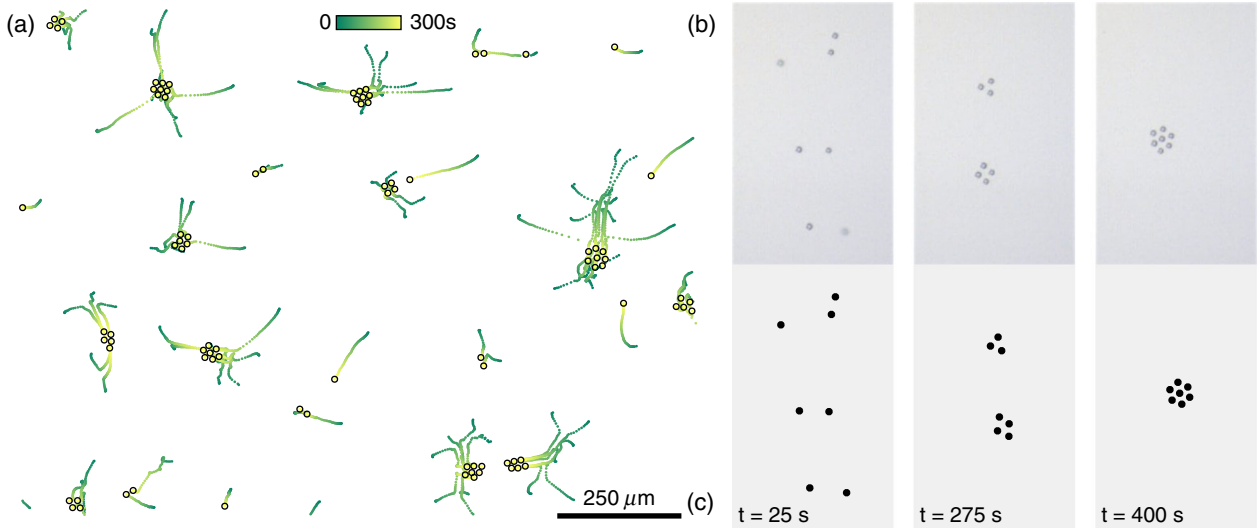

FIG. 3. Dynamics of assembly. (a) Experimental particle traces and the configuration reached after 5 min (disks). (b),(c) Consecutive snapshots from experiment (b) and a single simulation run (c) showing the formation of two clusters in their ground state (middle) and a large cluster with $n = 7$ particles (right). The simulations have been initialized with the positions extracted from the first experimental snapshot.

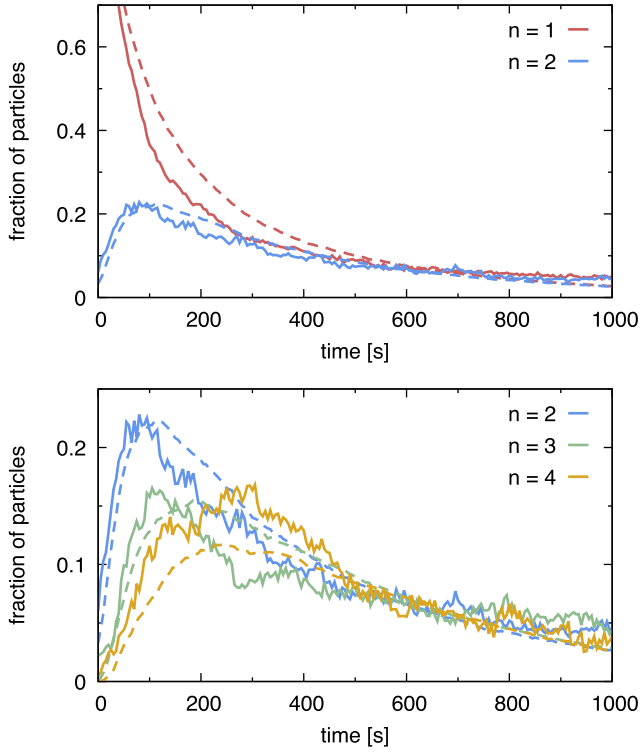

FIG. 4. Time evolution of cluster populations $N_n(t)/N$. Solid lines correspond to experimental data (averaged over several experiments), dashed lines to the simulation results of the theoretical model with $N = 80$ particles.

conservative potential. However, for larger aggregates, also the flow increases, leading to deviations from the predicted behavior (e.g., particles are lifted and pushed into the second layer). With even larger flows, particles are observed to spontaneously break the flow symmetry and become self-propelled. Another strategy is to explicitly break symmetry through mixtures of particles with different sizes or shapes or mixtures of activated and passive particles [33]. Here we explore the consequences of adding anionic ion exchange particles of similar size but releasing OH^- ions, for which we again observe the assembly of low-weight clusters. This is shown exemplary in Fig. 5 for two cationic particles and one anionic particle, which assemble into a trimer. As predicted in Ref. [22], the geometry together with the different mobilities or activities leads to a self-propelled complex. This can be seen through determining the center-of-mass speed of the three particles, which clearly shows a transition to a constant speed once the trimer has assembled.

In conclusion, we have shown that ion exchange particles close to a charged substrate generate flows that lead to effectively conservative, long-range interactions. Autonomous flow-driven assembly through long-range attractions might enable novel nonequilibrium materials and strategies in self-assembly, in particular, on intermediate scales for which thermal motion has become negligible but

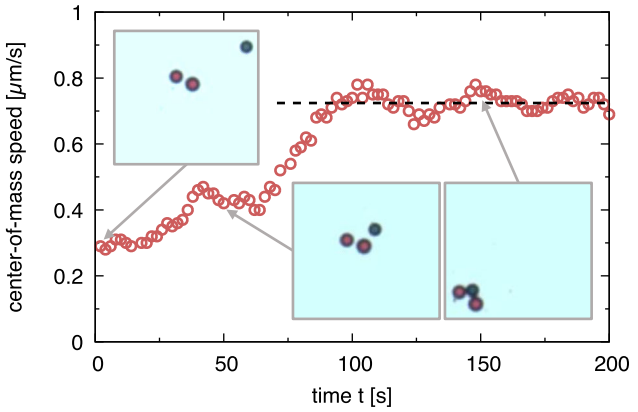

FIG. 5. Transition to self-propelled motion. Plotted is the center-of-mass speed of three particles, two cationic and one anionic, which accelerate once assembled into a trimer (at $t \approx 50$ s). For times $t = 0$, 50, and 150 s, snapshots are shown with cationic particles in red and anionic particles in blue. The field of view is the same for all snapshots. The dashed line indicates the final speed of the trimer.

which cannot be manipulated directly. Moreover, through changing composition, one may break the reciprocality of flow and particle mobility, resulting in directed motion. Previously, the directed motion of colloidal particles in combination with volume exclusion has been shown to lead to fascinating dynamic behavior ranging from clustering [34] and the formation of "living crystals" [35] to schooling and swarming [36]. Our results demonstrate how one can implement strategies to control and engineer interactions and directed motion on the same footing [37], which is a step towards designing active particles that can perform dynamical tasks such as the transport of cargo [38,39]. Concerning the size of the particles used here, we note that, in principle, smaller particles are possible, the main issue being the ion exchange rate and ion capacity of single particles that determines the flow strength and the time over which the flow is being generated [28].

We acknowledge the DFG for funding within the priority program SPP 1726 (Grants No. PA 459/18-1 and No. SP 1382/3-1).

[1] D. G. A. L. Aarts, M. Schmidt, and H. N. W. Lekkerkerker, Direct visual observation of thermal capillary waves, Science **304**, 847 (2004).

[2] T. Palberg, Crystallization kinetics of colloidal model suspensions: recent achievements and new perspectives, J. Phys. Condens. Matter **26**, 333101 (2014).

[3] C. P. Royall, M. E. Leunissen, and A. van Blaaderen, A new colloidal model system to study long-range interactions quantitatively in real space, J. Phys. Condens. Matter **15**, S3581 (2003).

[4] A. Yethiraj, Tunable colloids: Control of colloidal phase transitions with tunable interactions, Soft Matter **3**, 1099 (2007).
[5] G. Meng, N. Arkus, M. P. Brenner, and V. N. Manoharan, The free-energy landscape of clusters of attractive hard spheres, Science **327**, 560 (2010).
[6] R. W. Perry, M. C. Holmes-Cerfon, M. P. Brenner, and V. N. Manoharan, Two-Dimensional Clusters of Colloidal Spheres: Ground States, Excited States, and Structural Rearrangements, Phys. Rev. Lett. **114**, 228301 (2015).
[7] A. F. Demirörs, J. C. P. Stiefelhagen, T. Vissers, F. Smallenburg, M. Dijkstra, A. Imhof, and A. van Blaaderen, Long-Ranged Oppositely Charged Interactions for Designing New Types of Colloidal Clusters, Phys. Rev. X **5**, 021012 (2015).
[8] V. N. Manoharan, M. T. Elsesser, and D. J. Pine, Dense packing and symmetry in small clusters of microspheres, Science **301**, 483 (2003).
[9] S. Sacanna, W. T. M. Irvine, P. M. Chaikin, and D. J. Pine, Lock and key colloids, Nature (London) **464**, 575 (2010).
[10] M. E. Leunissen, C. G. Christova, A.-P. Hynninen, C. P. Royall, A. I. Campbell, A. Imhof, M. Dijkstra, R. van Roij, and A. van Blaaderen, Ionic colloidal crystals of oppositely charged particles, Nature (London) **437**, 235 (2005).
[11] B. de Nijs, S. Dussi, F. Smallenburg, J. D. Meeldijk, D. J. Groenendijk, L. Filion, A. Imhof, A. van Blaaderen, and M. Dijkstra, Entropy-driven formation of large icosahedral colloidal clusters by spherical confinement, Nat. Mater. **14**, 56 (2015).
[12] S. C. Glotzer and M. J. Solomon, Anisotropy of building blocks and their assembly into complex structures, Nat. Mater. **6**, 557 (2007).
[13] V. N. Manoharan, Colloidal matter: Packing, geometry, and entropy, Science **349**, 1253751 (2015).
[14] A. Campa, T. Dauxois, and S. Ruffo, Statistical mechanics and dynamics of solvable models with long-range interactions, Phys. Rep. **480**, 57 (2009).
[15] F. Ghezzi and J. C. Earnshaw, Formation of meso-structures in colloidal monolayers, J. Phys. Condens. Matter **9**, L517 (1997).
[16] K. D. Danov and P. A. Kralchevsky, Capillary forces between particles at a liquid interface: General theoretical approach and interactions between capillary multipoles, Adv. Colloid Interface Sci. **154**, 91 (2010).
[17] J. Bleibel, S. Dietrich, A. Domínguez, and M. Oettel, Shock Waves in Capillary Collapse of Colloids: A Model System for Two-Dimensional Screened Newtonian Gravity, Phys. Rev. Lett. **107**, 128302 (2011).
[18] K. Zahn, R. Lenke, and G. Maret, Two-Stage Melting of Paramagnetic Colloidal Crystals in Two Dimensions, Phys. Rev. Lett. **82**, 2721 (1999).
[19] F. Smallenburg, H. R. Vutukuri, A. Imhof, A. van Blaaderen, and M. Dijkstra, Self-assembly of colloidal particles into strings in a homogeneous external electric or magnetic field, J. Phys. Condens. Matter **24**, 464113 (2012).
[20] E. O. Budrene and H. C. Berg, Complex patterns formed by motile cells of escherichia coli, Nature (London) **349**, 630 (1991).
[21] C. Hertlein, L. Helden, A. Gambassi, S. Dietrich, and C. Bechinger, Direct measurement of critical casimir forces, Nature (London) **451**, 172 (2008).
[22] R. Soto and R. Golestanian, Self-Assembly of Catalytically Active Colloidal Molecules: Tailoring Activity through Surface Chemistry, Phys. Rev. Lett. **112**, 068301 (2014).
[23] R. Soto and R. Golestanian, Self-assembly of active colloidal molecules with dynamic function, Phys. Rev. E **91**, 052304 (2015).
[24] A. Banerjee, I. Williams, R. N. Azevedo, M. E. Helgeson, and T. M. Squires, Soluto-inertial phenomena: Designing long-range, long-lasting, surface-specific interactions in suspensions, Proc. Natl. Acad. Sci. U.S.A. **113**, 8612 (2016).
[25] D. Feldmann, S. R. Maduar, M. Santer, N. Lomadze, O. I. Vinogradova, and S. Santer, Manipulation of small particles at solid liquid interface: Light driven diffusioosmosis, Sci. Rep. **6**, 36443 (2016).
[26] J. L. Anderson, Colloid transport by interfacial forces, Annu. Rev. Fluid Mech. **21**, 61 (1989).
[27] R. Niu, P. Kreissl, A. T. Brown, G. Rempfer, D. Botin, C. Holm, T. Palberg, and J. de Graaf, Microfluidic pumping by micromolar salt concentrations, Soft Matter **13**, 1505 (2017).
[28] See Supplemental Material at http://link.aps.org/supplemental/10.1103/PhysRevLett.119.028001 for a detailed description of the experiments, measurements of *p*H and the ion exchange rate, a calculation of the bond vibrations, and more details on the observed structures (citing Refs. [6, 27, 29]) as well as supporting movies.
[29] A. Malins, S. R. Williams, J. Eggers, and C. P. Royall, Identification of structure in condensed matter with the topological cluster classification, J. Chem. Phys. **139**, 234506 (2013).
[30] S. Ebbens, R. A. L. Jones, A. J. Ryan, R. Golestanian, and J. R. Howse, Self-assembled autonomous runners and tumblers, Phys. Rev. E **82**, 015304 (2010).
[31] S. Ni, E. Marini, I. Buttinoni, H. Wolf, and L. Isa, Rational design and fabrication of versatile active colloidal molecules, arXiv:1701.08061.
[32] D. Aldous, Deterministic and stochastic models for coalescence (aggregation and coagulation): A review of the mean-field theory for probabilists, Bernoulli **5**, 3 (1999).
[33] A. Reinmüller, H. J. Schöpe, and T. Palberg, Self-organized cooperative swimming at low Reynolds numbers, Langmuir **29**, 1738 (2013).
[34] I. Buttinoni, J. Bialké, F. Kümmel, H. Löwen, C. Bechinger, and T. Speck, Dynamical Clustering and Phase Separation in Suspensions of Self-Propelled Colloidal Particles, Phys. Rev. Lett. **110**, 238301 (2013).
[35] J. Palacci, S. Sacanna, A. P. Steinberg, D. J. Pine, and P. M. Chaikin, Living crystals of light-activated colloidal surfers, Science **339**, 936 (2013).
[36] J. Yan, M. Han, J. Zhang, C. Xu, E. Luijten, and S. Granick, Reconfiguring active particles by electrostatic imbalance, Nat. Mater. **15**, 1095 (2016).
[37] J. Zhang, J. Yan, and S. Granick, Directed self-assembly pathways of active colloidal clusters, Angew. Chem., Int. Ed. **55**, 5166 (2016).
[38] S. Sundararajan, P. E. Lammert, A. W. Zudans, V. H. Crespi, and A. Sen, Catalytic motors for transport of colloidal cargo, Nano Lett. **8**, 1271 (2008).
[39] L. Baraban, M. Tasinkevych, M. N. Popescu, S. Sanchez, S. Dietrich, and O. G. Schmidt, Transport of cargo by catalytic Janus micro-motors, Soft Matter **8**, 48 (2012).